

Detailed study of extended gamma-ray morphology in the vicinity of the Coma cluster with *Fermi*-LAT

Vardan Baghmanyany,¹★ Davit Zargaryan,^{2,3}† Felix Aharonian,^{2,3,4} Ruizhi Yang,⁵ Sabrina Casanova^{1,4} and Jonathan Mackey^{2,3}

¹*Institute of Nuclear Physics PAN, Radzikowskiego 152, 31-342 Kraków, Poland*

²*Dublin Institute for Advanced Studies, 31 Fitzwilliam Place, Dublin 2, Ireland*

³*Centre for AstroParticle Physics and Astrophysics, DIAS Dunsink Observatory, Dunsink Lane, Dublin 15, Ireland*

⁴*Max-Planck-Institut für Kernphysik, P.O. Box 103980, 69029 Heidelberg, Germany*

⁵*Department of Astronomy, School of Physical Sciences, University of Science and Technology of China, Hefei, Anhui 230026, China*

Accepted XXX. Received YYY; in original form ZZZ

ABSTRACT

Context. Galaxy clusters can be sources of high energy (HE) γ -ray radiation due to the efficient acceleration of particles up to the highest energies. Up to now, the only candidate of emitting γ -rays is the Coma cluster, towards which there is an excess of the γ -ray emission detected by the *Fermi* Large Area Telescope (LAT).

Aims. In particular, we aim to understand the origin of this excess and its connection with the Coma cluster.

Methods. Using ~ 12.3 years of *Fermi*-LAT data, we analysed the region of the Coma cluster between energies 100 MeV and 1 TeV by detailed spectral and morphological analysis.

Results. We detected a diffuse γ -ray emission between 100 MeV and 1 TeV energies in the region of the Coma cluster with 5.4σ extension significance and 68% containment radius of $0.82^{+0.1}_{-0.05}$ degrees derived with a 2D homogeneous disk model. The corresponding γ -ray spectrum extends up to ~ 50 GeV with power-law spectral index $\Gamma = 2.23 \pm 0.11$ and energy flux of $(3.48 \pm 0.68) \times 10^{-12}$ erg cm⁻² s⁻¹. Besides, we also found that three point-like sources in the background with power-law indexes of 2.44 ± 0.28 , 2.56 ± 0.32 , and 1.99 ± 0.30 show improvement in the fit by $\Delta_{\text{AIC}} = -7.2$.

Conclusions. We suggest that the observed γ -ray emission can be produced within the Coma cluster since the contribution from the background AGNs and star-forming galaxies is not sufficient to provide the observed total γ -ray luminosity and the morphology. However, to confirm this suggestion, we need more data because of the low statistics of each component in the model.

Key words: methods: data analysis - clusters: Coma cluster - gamma-rays: galaxies: clusters

1 INTRODUCTION

Clusters of Galaxies are the largest gravitationally bound astrophysical structures in the Universe. They are essential cosmological laboratories for studying a variety of astronomical phenomena, e.g., star formation, the interaction of galaxies, gravity, particle acceleration, etc. (Völk et al. 1996). The linear scale of galaxy clusters can extend several Mpc (angular scale of a few degrees). They consist of sometimes thousands of galaxies surrounded by hot and diffuse intracluster gas. Radio observations of clusters of galaxies have revealed the existence of diffuse structures with a regular and

irregular shape, so-called radio halo and relic, with non-thermal spectra implying significant energy density in accelerated particles (Giovannini et al. 1993; Giovannini & Feretti 2000). The magnetic field strength within the cluster is around a few μG (Carilli & Taylor 2002; Govoni & Feretti 2004), which leads to inefficient diffusion of cosmic rays (CRs). Therefore, galaxy clusters can retain accelerated particles for cosmologically long timescales, which can thus be accumulated within a cluster and produce detectable high energy (HE) emission through collision with ambient matter (Völk et al. 1996; Berezhinsky et al. 1997).

A number of astrophysical sources can be responsible for the production and the acceleration of CRs in galaxy clusters. Supernova-driven galactic winds are considered as potential candidates (Völk et al. 1996), and studies have shown that AGNs located

★ E-mail: vardan.baghmanyany@ifj.edu.pl

† E-mail: dzargaryan@cp.dias.ie

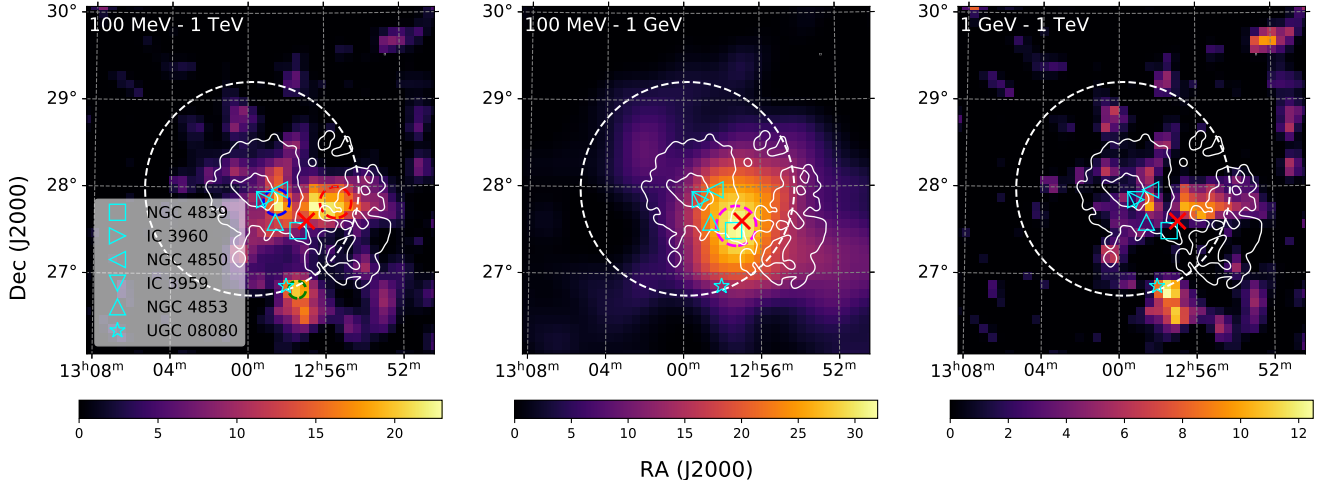


Figure 1. TS map of a $4^\circ \times 4^\circ$ region centred on the Coma cluster (left: the whole energy range, middle: 100 MeV - 1 TeV, right: 1 GeV - 1 TeV) generated with *tmap* tool assuming a power-law point source with $\Gamma = 2$. The dashed white circle represents the virial region of the Coma cluster ($\theta_{200} = 1.23^\circ$). The solid white-colored contours express the radio measurements of the halo and the relic of the Coma cluster with the Westerbork Synthesis Telescope (WSRT) telescope at 352 MHz (Brown & Rudnick 2011). The cyan-colored markers represent different types of AGNs in the region with NASA/IPAC Extragalactic Data (NED) positions, and the red marker shows the location of the 4FGL J1256.9+2736 source from the *Fermi*-LAT 4FGL-DR2 catalog. The blue, red, and green colored dashed circles in the left panel and magenta dashed circle in the middle panel correspond to the 68% containment regions of point-like sources around p_1 , p_2 , p_3 , and p_{low} , respectively.

in galaxy clusters could significantly contribute to CRs (Ensslin et al. 1997; Aharonian 2002; Hinton et al. 2007). Furthermore, large-scale intergalactic shocks, generated by the accretion and merger processes (Colafrancesco & Blasi 1998; Ryu et al. 2003; Gabici & Blasi 2003b, 2004) and turbulent re-acceleration (Brunetti & Blasi 2005) have been proposed as acceleration sites.

Studying clusters of galaxies in the γ -ray band is challenging but can provide important constraints on the efficiency of particle acceleration, magnetic confinement, and radiation processes of CRs (Blasi et al. 2007). The accelerated CRs can produce HE γ -rays through leptonic and hadronic radiative processes. In the hadronic scenario, the inelastic collision of accelerated CR protons with the thermal nuclei in the intra-cluster medium could produce γ -rays via pion decay (Dennison 1980). For the leptonic scenario, ultra-relativistic electrons up-scatter target photon fields (e.g., cosmic microwave background (CMB), infrared background) to HE γ -rays (Atoyan & Völk 2000; Gabici & Blasi 2003a). Alternatively, γ -ray production may be either from inverse Compton (IC) scattering by secondary electrons in Bethe-Heitler processes, when relativistic protons interact with CMB photon field (Inoue et al. 2005; Kelner & Aharonian 2008). Another possibility is synchrotron radiation of ultra-relativistic electrons, which originate from the interactions of VHE γ -rays with diffuse extragalactic background radiation field (Timokhin et al. 2004). Hadronic γ -ray emission is more likely in galaxy clusters than leptonic emission because accelerated HE electrons have relatively short lifetimes (due to energy losses) and do not accumulate to the same extent as protons. As a result, their spectrum can be characterized by an early cut-off below the HE regime (Atoyan & Völk 2000).

The Coma galaxy cluster (Abell 1656) is considered a unique astronomical laboratory because of its proximity ($z = 0.023$; Struble & Rood 1991) and high total mass ($M_{500} \approx 6 \times 10^{14} M_\odot$; Planck Collaboration et al. 2013). It has been intensively investigated over the past decades in all wavebands, i.e. from radio to very (HE) γ -rays. The radio observations of Coma Cluster have revealed an extended, non-thermal, radio halo associated with the cluster core

(Large et al. 1959; Willson 1970; Giovannini et al. 1993; Thierbach et al. 2003; Brown & Rudnick 2011; van Weeren et al. 2019) and a diffuse radio relic with an extension of ~ 2 Mpc at approximately the virial radius (Jaffe & Rudnick 1979; Deiss et al. 1997; Brown & Rudnick 2011). Also, Kronberg et al. (2007) have investigated a ~ 4 Mpc diameter of diffuse radio structure around Coma Cluster.

The recent X-ray observations showed a complex morphology towards the Coma cluster, such as a sub-group in the South-West part of the cluster connected to NGC 4839 and another sub-structure between the center of the Coma cluster and NGC 4839 (Neumann et al. 2003). Also, X-ray observations revealed various evidence of infall of galaxies, such as the group of NGC 4839 (e.g. Neumann et al. 2001; Malavasi et al. 2020). More recently, the X-ray observation of the Coma cluster with the SRG/eROSITA telescope revealed a rich structure extending up to the virial radius of the cluster (Churazov et al. 2021). They explained this by a recent merging of the Coma cluster with the NGC 4839 group indicated by the detected faint X-ray bridge, which connects the galaxy group with the cluster.

In the HE γ -ray band, the Coma cluster was first studied by *Fermi*-LAT using six years of data, showing two low significance structures within the virial radius (Ackermann et al. 2016). Then using more data of *Fermi*-LAT, Xi et al. (2018) detected extended γ -ray emission from the direction of the Coma cluster in the 0.2-300 GeV band characterized with a soft spectral index of $\Gamma \sim 2.7$. The detection of HE γ -ray excess towards the Coma cluster with *Fermi*-LAT data was confirmed by Adam et al. (2021), where the total γ -ray emission was explained by hadronic interactions in the intracluster gas.

In this paper, we present a detailed investigation of γ -ray emission in the direction of the Coma cluster using more than 12 years of *Fermi*-LAT data. In Section 2, we describe the details of the *Fermi*-LAT data analysis and, in section 3, we report the results. Finally, in Section 4, the discussion and conclusion of this work are presented.

Table 1. The results of the morphological analysis of the Coma cluster region with the corresponding statistical errors. The second to fifth columns show the localised positions, position uncertainties at 68% (R_{68}^{pos}), and TS values of all morphological components. The 68% containment radii (R_{68}) and extension TS values (TS_{ext}) of the models used in the extension analysis are given in the sixth and seventh columns, respectively.

| Spatial model | RA _{J2000} [deg] | Dec _{J2000} [deg] | R_{68}^{pos} [deg] | TS | R_{68} [deg] | TS_{ext} |
|-----------------------|------------------------------|-------------------------------|--------------------------------|------|------------------------|--------------------------|
| RadialDisk | 194.14 ± 0.14 | 27.38 ± 0.13 | 0.19 | 51.6 | $0.82^{+0.10}_{-0.05}$ | 29.3 |
| RadialGaussian | 194.27 ± 0.17 | 27.56 ± 0.17 | 0.26 | 50.2 | $0.91^{+0.18}_{-0.16}$ | 9.8 |
| P1 + P2 + P3 | | | | | | |
| p1 | 194.63 ± 0.08 | 27.83 ± 0.13 | 0.15 | 17.2 | - | - |
| p2 | 193.86 ± 0.15 | 27.82 ± 0.10 | 0.18 | 16.4 | - | - |
| p3 | 194.37 ± 0.06 | 26.82 ± 0.07 | 0.10 | 15.4 | - | - |

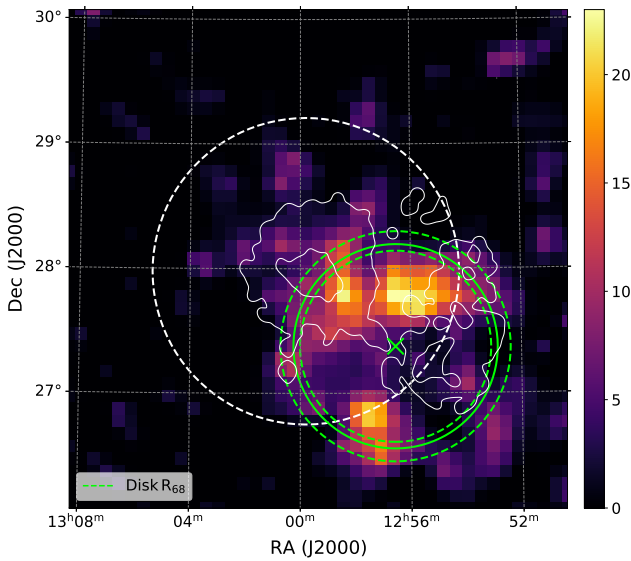


Figure 2. TS map of the Coma cluster region in the energy range between 100 MeV and 1 TeV. The 2D homogeneous disk model represented by the 68% containment radius is shown in a solid green circle with the corresponding 1σ statistical errors marked by green dashed circles.

2 FERMI-LAT DATA ANALYSIS

2.1 Data selection and background models

We used 12.3 years (August 4, 2008 - June 1, 2021) of *Fermi*-LAT Pass 8 ULTRACLEANVETO (‘FRONT + BACK’) class events (Atwood et al. 2013). The selection of this event class was on account of the lowest level of CR contamination, that makes this class ideal for diffuse emission study, which is the main goal of this analysis. The data selection was within a region of interest (ROI) of 12° around the center of the Coma cluster at R.A., Dec = (194.95, 27.98) between 100 MeV and 1 TeV energies. We analysed the data with Fermipy (version 1.0.0; Wood et al. 2017) and *Fermitools* software packages v2.0.0¹ following the standard procedure of the binned maximum-likelihood analysis technique with the P8R3_ULTRACLEANVETO_V3 instrument response functions (IRFs). The data reduction was performed by using the recommended (DATA_QUAL > 0)&&(LAT_CONFIG == 1) data quality filters. And to reduce the contamination from the Earth’s atmosphere, we employed a zenith angle cut of 90° to the events.

¹ <https://github.com/fermi-lat/Fermitools-conda/wiki>

In the spatial binning, we applied a pixel size of 0.1° and nine logarithmic energy bins per decade for the spectral binning. In the construction of the sky model, we used *Fermi*-LAT sources from the second incremental version of the fourth catalog (4FGL-DR2; Ballet et al. 2020, Abdollahi et al. 2020) lying up to 5° beyond the ROI. To account for the diffuse emission, we modeled the Galactic diffuse emission model (gll_iem_v07.fits) with isotropic component (iso_P8R3_ULTRACLEANVETO_V3_v1.txt) relevant to the ULTRACLEANVETO event class.

2.2 Morphological and spectral analysis

The detection of γ -ray emission from the direction of the Coma cluster has been already reported and studied by several authors using different spatial models (Xi et al. 2018; Adam et al. 2021; Zargaryan et al. 2021). The excess γ -ray emission at (R.A., Dec) = (194.24, 27.61) degrees has been also added to the 4FGL-DR2 catalog as a point source named 4FGL J1256.9+2736 with power-law spectral index $\Gamma = 2.73$. To study this excess, we analysed the data for 100 MeV-1 TeV, 100 MeV-1 GeV, and 1 GeV-1 TeV energy bands by removing 4FGL J1256.9+2736 from the source list as a baseline model. In the fitting, the spectral parameters of sources inside the ROI were left free, while for the sources outside the ROI, we used their 4FGL values, keeping them fixed during the fit. For all sources besides the diffuse background models, we applied the energy dispersion correction. After the first iteration of the fit, we removed sources with a test statistic (TS)² lower than 1 and repeated the fitting until no source with $\text{TS} < 1$ was found. Then, we added the significant peaks above $\text{TS}=16$ beyond the 2° from the ROI center to the model using *find_sources* tool implemented in Fermipy. This tool uses an iterative maximum-likelihood algorithm that creates a TS map of the ROI for the given model, identifies the significant peaks as new sources with the corresponding peak positions, and adds them to the model by repeatedly fitting. This process repeats until no peak is found above the given threshold. The TS maps of the resulting baseline models in the energy ranges of 100 MeV - 1 TeV, 100 MeV-1 GeV, and 1 GeV-1 TeV are shown in Figure 1 within $4^\circ \times 4^\circ$ around the center of the Coma cluster.

It is easy to see that in the TS map of the whole energy range (shown in the left panel of Figure 1) there are three point-like structures identified on top of the excess diffuse emission. This residual structure remains the same in the TS map of the higher energy range

² TS is defined as twice of the difference between the log-likelihoods of source plus background (\mathcal{L}_1) and only background as a null hypothesis (\mathcal{L}_0): $\text{TS} = 2\log(\mathcal{L}_1/\mathcal{L}_0)$.

Table 2. A summary of spectral analysis results. The $\log(\mathcal{L})_{\max}$ values, listed in the sixth column, are returned from the binned maximum-likelihood analysis between 100 MeV and 1 TeV range. Δ_{AIC} and N_{dof} values in the seventh and eighth columns refer to the AIC values and degrees of freedom relative to the uniform disk model, respectively.

| Spatial model | Energy flux [$10^{-12} \times \text{erg cm}^{-2} \text{s}^{-1}$] | Index | TS | N_{pred} | $\log(\mathcal{L})_{\max}$ | Δ_{AIC} | N_{dof} |
|--|---|-----------------|------|-------------------|----------------------------|-----------------------|------------------|
| Disk | 3.84 ± 0.67 | 2.23 ± 0.11 | 51.6 | 863.2 | -313141.3 | - | |
| $p_1 + p_2 + p_3$ | | | | | -313135.0 | -4.7 | 4 |
| p_1 | 1.05 ± 0.37 | 2.47 ± 0.23 | 17.2 | 330.8 | | | |
| p_2 | 1.16 ± 0.39 | 2.53 ± 0.24 | 16.4 | 388.0 | | | |
| p_3 | 0.93 ± 0.35 | 2.08 ± 0.24 | 15.4 | 151.7 | | | |
| Disk + $p_1 + p_2 + p_3$ | | | | | -313131.7 | -7.2 | 6 |
| Disk | 1.54 ± 1.06 | 2.09 ± 0.26 | 5.6 | 250.2 | | | |
| p_1 | 0.82 ± 0.37 | 2.44 ± 0.28 | 11.1 | 249.7 | | | |
| p_2 | 0.86 ± 0.43 | 2.56 ± 0.32 | 8.8 | 289.3 | | | |
| p_3 | 0.75 ± 0.39 | 1.99 ± 0.30 | 9.4 | 91.5 | | | |

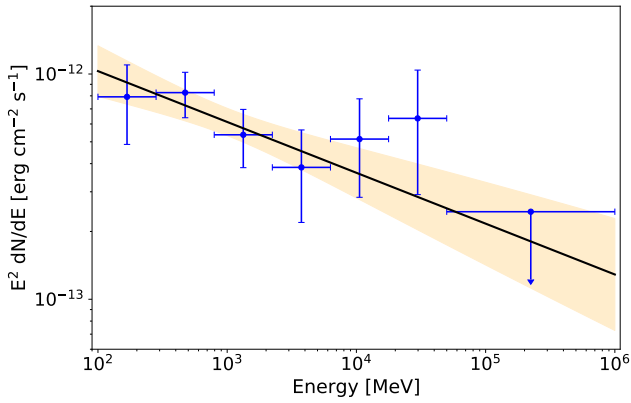


Figure 3. The SED of the excess γ -ray emission from the region of the Coma cluster derived from the only disk model, where the shaded orange area marks the 1σ errors on the fitted spectral model. The ULs are computed at 95% CL for the energy bins below 2σ .

(1 GeV - 1 TeV) with lower significance (see right panel of Figure 1). These point-like sources were also identified with *find_sources* tool at localised positions of (R.A., Dec) = (194.63, 27.83) degrees, (R.A., Dec) = (193.86, 27.82) degrees, and (R.A., Dec) = (194.37, 26.82) degrees with detection significances above $\sim 4\sigma$. Hereafter, these point-like sources will be referred to as p_1 , p_2 , and p_3 , respectively, while the corresponding joint spatial model as $p_1 + p_2 + p_3$. The 68% containment regions of p_1 , p_2 and p_3 are shown in the left panel of Figure 1 by blue, red and green dashed circles, respectively. The middle panel of Figure 1 shows the TS map of the lower energy range between 100 MeV - 1 GeV, where the dashed magenta circle represents the 68% containment region around the peak (hereafter p_{low}).

To test the extension of the excess γ -ray emission for the whole energy range of our analysis, we used the *extension* tool in *Fermipy*. This tool computes TS of the extension hypothesis defined as $\text{TS}_{\text{ext}} = 2 \times (\log \mathcal{L}_{\text{ext}} - \log \mathcal{L}_{\text{PS}})$, where $\log \mathcal{L}_{\text{ext}}$ and $\log \mathcal{L}_{\text{PS}}$ are likelihood values of the extended and point-like source models, respectively. As an input, we used the localised position of 4FGL J1256.9+2736 estimated with the *localize* tool in *Fermipy* after adding it into the baseline model. We checked the source extension for 2D Gaussian and 2D uniform-disk models, in both cases assuming a power-law spectral model. During the fitting, we left

the position and the spectral parameters of the testing source and the normalization of all sources within 5° from the center of ROI to vary. For the 2D uniform disk model we obtained $\text{TS}_{\text{ext}} \sim 29.3$ with 68% containment radius of $R_{68} = 0.82^{+0.10}_{-0.05}$, while for the 2D symmetric Gaussian model no significant extension was detected ($\text{TS}_{\text{ext}} \sim 9.8$). The results of the extension analysis are summarized in Table 1 and the detected extension with a uniform disk model is shown in Figure 2.

Lastly, with the 2D uniform disk model obtained from the extension analysis, we also included the peak-like sources with localised positions assuming the power-law model on all components. The fitting was performed by following the procedure described in the previous section. This model hereafter will be referred to as disk + $p_1 + p_2 + p_3$.

3 RESULTS

The total spectral energy distribution (SED) of the Coma cluster region for the only disk model is shown in Figure 3. It is well fitted with a power-law index of $\Gamma = 2.23 \pm 0.11$ and energy flux ($F_\gamma = 3.48 \pm 0.68$) $\times 10^{-12} \text{ erg cm}^{-2} \text{ s}^{-1}$, which is compatible with the total fluxes of the best models obtained in Xi et al. (2018) and Adam et al. (2021). The spectral index is much harder than the index of extended radio component of the favored radio+p1 model found in Xi et al. (2018), while it is compatible with the index of p_1 component ($\Gamma = 2.22 \pm 0.27$). It is also similar to the spectral index ($\Gamma \sim 2.3$) used in Ackermann et al. (2016) in the computation of upper limits (ULs).

The best-fit parameters of the models, described in the previous section, are given in Table 2 with the corresponding log-likelihood ($\log \mathcal{L}$), and the Akaike information criterion (AIC, (Akaike 1974)) values. The AIC is defined as $\text{AIC} = 2(\Delta \text{d.o.f.} - \Delta \log \mathcal{L})$, where the difference between the number of degrees of freedom (DOF) ($\Delta \text{d.o.f.}$) and the log-likelihood ($\Delta \log \mathcal{L}$) values are computed relative to the homogeneous disk model. In this formulation, the model with the smallest AIC value is considered as the favored model. However, it should be noted that the AIC method does not allow estimating the significance of the differences between tested models relative to each other.

Following the estimations of AIC values listed in Table 2, we can see that disk + $p_1 + p_2 + p_3$ is the best-model with $\text{AIC} = -7.2$ preference over the homogeneous disk model. This indicates that

besides the disk component that has $\Gamma = 2.09 \pm 0.26$ spectral index in this model, there are two point-like structures inside the virial radius of the Coma cluster around p_1 and p_2 , which are described with softer power-law indices of $\Gamma = 2.44 \pm 0.28$ and $\Gamma = 2.56 \pm 0.32$, respectively. The spectral index of the third point-like excess around p_3 , that is out of the virial radius, is rather hard $\Gamma = 1.99 \pm 0.30$, which is compatible with the spectrum of the disk component. We note that these point-like structures are still visible in the significance map between 1 GeV–1 TeV (see right panel of Figure 1) with $> 3\sigma$ significances at peak positions. We also analysed the excess γ -ray emission between 100 MeV and 1 GeV shown in the middle panel of Figure 1 by assuming a point-like source at the position of p_{low} . It resulted in TS = 36 detection with a hard power-law spectral index of $\Gamma = 1.95 \pm 0.42$.

Taking into account the low significances of all components in disk + p_1 + p_2 + p_3 model, we performed spectral analysis on 1000 simulated datasets between 100 MeV and 1 TeV using the best-fit parameters of this model as initial values (see Appendix A for more detailed description). The resulting distribution of spectral indices, energy fluxes, and TS values are shown in Figure 4 for all components in comparison with the input values of disk + p_1 + p_2 + p_3 model indicated by dashed lines. The standard independent 2-sample t-test on the resulting distributions of spectral indices of the disk model with the point-like components shows significant anticorrelation with $< 9 \times 10^{-6}$ probability. This confirms the results of the AIC test indicating additional sources of γ -ray emission besides the disk model. We also evaluated the systematic uncertainties in the spectral parameters due to the Galactic interstellar emission model (IEM) and the choice of the event class, which can be found in Table 3. The systematic uncertainties on the spectral indices for all components due to the selection of IEM are $< 8\%$, while the flux uncertainty on the disk component reaches up to $\sim 76\%$ and no more than $\sim 28\%$ for the other components. The systematic errors coming from the selection of event classes are estimated to be $< 12\%$ on the energy flux and $< 8\%$ on the spectra index of all components in the model.

4 DISCUSSION AND CONCLUSION

We have presented the detection of diffuse γ -ray emission in the vicinity of the Coma cluster with $\sim 5.4\sigma$ extension significance modeled as a 2D homogeneous disk. The localised position of the extension center (RA = 194.14 ± 0.14 , Dec = 27.38 ± 0.13 degrees) has an offset of 0.94° from the center of the virial region of the Coma cluster, while the radius $r = 1.0^{+0.12}_{-0.06}$ degrees ($r = R_{68}/0.82$) is compatible with the virial radius ($\Theta_{200} = 1.23^\circ$). The corresponding spectrum of the excess extends up to ~ 50 GeV exhibiting a hard power-law spectrum with $\Gamma = 2.23 \pm 0.11$ and energy flux of $(3.48 \pm 0.68) \times 10^{-12} \text{ erg cm}^{-2} \text{ s}^{-1}$. Nevertheless, as shown by the AIC test, the presence of the point-like sources around p_1 , p_2 , and p_3 peaks in the model improve the fit. In particular, the spectral indices of point-like sources around p_1 and p_2 are $\Gamma = 2.54 \pm 0.28$ and $\Gamma = 2.56 \pm 0.32$, respectively, showing a hint of softening with respect to the disk component, $\Gamma = 2.09 \pm 0.26$. As we discussed in the previous section, the t-test shows that the spectral indices of p_1 and p_2 as well as p_3 show significant anti-correlation compared to the disk component. This indicates that the extended emission may have a contribution from the emission of compact sources, such as radiogalaxies and star-forming galaxies. The former was estimated by Ackermann et al. (2016) for the radio brightest of radiogalaxies NGC 4869 and NGC 4874 in the center of the Coma cluster according to Cordey (1985), both of are located at the periphery of

the 68% containment region of p_1 . The combined γ -ray luminosity was estimated to be $L_\gamma \sim 8 \times 10^{40} \text{ erg s}^{-1}$, assuming that the γ -ray emission is produced via IC scattering of CMB photons by radio-producing electrons (IC/CMB model). This is only the $\sim 8\%$ of the observed γ -ray luminosity from p_1 (assuming disk + p_1 + p_2 + p_3 model), which is $L_\gamma = (0.98 \pm 0.44) \times 10^{42} \text{ erg s}^{-1}$. Other radiogalaxies in the cluster and the background, such as IC 3960, IC 3959, and NGC 4850, have weaker radio fluxes; therefore, one can conclude that they can not be responsible for the whole observed γ -ray emission around the p_1 . In this regard, the situation is more clear for the γ -ray excess around the p_2 peak, which does not overlap with any radiogalaxy from the NED catalog. The association of the p_3 point-like source with the only background AGN UGC 08080 (the only AGN in the 68% containment radius of p_3) is hard to show since no radio data is available.

The expected γ -ray emission from star-forming galaxies in 0.1–100 GeV range was estimated by Storm et al. (2012) to be $L_\gamma \sim 3 \times 10^{40} - 3 \times 10^{42} \text{ erg s}^{-1}$ range. Taking into account the fact that the detected γ -ray emission has an extension of ~ 1.8 Mpc radius, it is less likely that star-forming galaxies can provide the observed morphology, even if the higher limit of the estimated γ -ray luminosity is on the order of the observed total γ -ray luminosity ($\sim 4.8 \times 10^{42} \text{ erg s}^{-1}$).

Very recently, Churazov et al. (2021) reported the first results of the X-ray studies of the Coma cluster SRG/eROSITA data. They revealed a complex morphology with two structures around the core and a faint X-ray bridge connecting the NGC 4839 group with the cluster. Based on this, they assume that the two extended X-ray features can be the results of a recent merger of the cluster with the NGC 4839 group as discussed in Zhang et al. (2021). Interestingly, that the γ -ray excess around p_1 (see the left panel of Figure 1) overlaps with a bow-like sharp X-ray feature found in Zhang et al. (2021). In contrast, the γ -ray excess associated with p_2 does not have any overlap with the X-ray morphology of the study discussed above. Also, we want to mention that the center of the γ -ray disk and the γ -ray morphology between 100 MeV and 1 GeV are located on top of the NGC 4839 group in the X-ray image.

All in all, our study shows that the extended γ -ray excess towards the Coma cluster is not homogeneous, showing several γ -ray compact structures around p_1 and p_2 . However, the poor angular resolution of *Fermi*-LAT, as well as the low statistics for all components in disk + p_1 + p_2 + p_3 model, does not allow us to confirm or reject the correlation with the X-ray morphology obtained by Zhang et al. (2021). An additional difficulty is that the γ -ray emission extends beyond the virial radius of the Coma cluster forming the point-like structure around p_3 whose origin is not clear. To summarize, more data of *Fermi*-LAT are needed to resolve the HE γ -ray morphology more carefully and check the viability of the model discussed in this work. In particular, the origin of the detected extension and its connection with the detected point-like structures requires a significant improvement in statistics, which would allow measuring their positions and the spectra more precisely.

ACKNOWLEDGEMENTS

DZ acknowledges funding from an Irish Research Council (IRC) Starting Laureate Award (IRCLA\2017\83). JM acknowledges support from a Royal Society-Science Foundation Ireland University Research Fellowship (14/RS-URF/3219, 20/RS-URF-R/3712) and an Irish Research Council (IRC) Starting Laureate Award (IR-

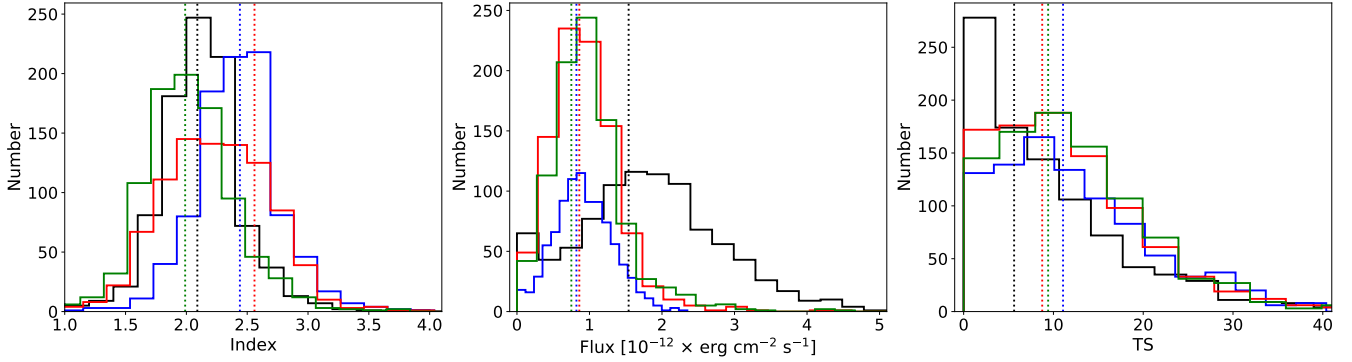


Figure 4. Distribution of spectral indices, energy fluxes, and TS values of disk (black), p_1 (blue), p_2 (red), and p_3 (green) components of the disk + p_1 + p_2 + p_3 model derived from the fitting of 1000 simulated datasets. The corresponding input parameters of all components used as inputs to the simulations are displayed in dashed lines with the same colors.

CLA\2017\83). SC acknowledges funding from the Polish Science Centre grant DEC-2017/27/B/ST9/02272.

REFERENCES

- Abdollahi S., et al., 2020, *ApJS*, **247**, 33
- Acero F., et al., 2016, *ApJS*, **224**, 8
- Ackermann M., et al., 2016, *ApJ*, **819**, 149
- Adam R., Goksu H., Brown S., Rudnick L., Ferrari C., 2021, *A&A*, **648**, A60
- Aharonian F. A., 2002, *MNRAS*, **332**, 215
- Akaike H., 1974, *IEEE Transactions on Automatic Control*, **19**, 716
- Atoyan A. M., Völk H. J., 2000, *ApJ*, **535**, 45
- Atwood W., et al., 2013, Pass 8: Toward the Full Realization of the Fermi-LAT Scientific Potential ([arXiv:1303.3514](https://arxiv.org/abs/1303.3514))
- Ballet J., Burnett T. H., Digel S. W., Lott B., 2020, *arXiv e-prints*, p. [arXiv:2005.11208](https://arxiv.org/abs/2005.11208)
- Berezinsky V. S., Blasi P., Ptuskin V. S., 1997, *ApJ*, **487**, 529
- Blasi P., Gabici S., Brunetti G., 2007, *International Journal of Modern Physics A*, **22**, 681
- Brown S., Rudnick L., 2011, *MNRAS*, **412**, 2
- Brunetti G., Blasi P., 2005, *MNRAS*, **363**, 1173
- Carilli C. L., Taylor G. B., 2002, *ARA&A*, **40**, 319
- Churazov E., Khabibullin I., Lyskova N., Sunyaev R., Bykov A. M., 2021, *A&A*, **651**, A41
- Colafrancesco S., Blasi P., 1998, *Astroparticle Physics*, **9**, 227
- Cordey R. A., 1985, *MNRAS*, **215**, 437
- Deiss B. M., Reich W., Lesch H., Wielebinski R., 1997, *A&A*, **321**, 55
- Dennison B., 1980, *ApJ*, **239**, L93
- Ensslin T. A., Biermann P. L., Kronberg P. P., Wu X.-P., 1997, *ApJ*, **477**, 560
- Gabici S., Blasi P., 2003a, *Astroparticle Physics*, **19**, 679
- Gabici S., Blasi P., 2003b, *ApJ*, **583**, 695
- Gabici S., Blasi P., 2004, *Astroparticle Physics*, **20**, 579
- Giovannini G., Feretti L., 2000, *New Astron.*, **5**, 335
- Giovannini G., Feretti L., Venturi T., Kim K. T., Kronberg P. P., 1993, *ApJ*, **406**, 399
- Govoni F., Feretti L., 2004, *International Journal of Modern Physics D*, **13**, 1549
- Hinton J. A., Domainko W., Pope E. C. D., 2007, *MNRAS*, **382**, 466
- Inoue S., Aharonian F. A., Sugiyama N., 2005, *ApJ*, **628**, L9
- Jaffe W. J., Rudnick L., 1979, *ApJ*, **233**, 453
- Kelner S. R., Aharonian F. A., 2008, *Phys. Rev. D*, **78**, 034013
- Kronberg P. P., Kothes R., Salter C. J., Perillat P., 2007, *ApJ*, **659**, 267
- Large M. I., Mathewson D. S., Haslam C. G. T., 1959, *Nature*, **183**, 1663
- Malavasi N., Aghanim N., Tanimura H., Bonjean V., Douspis M., 2020, *A&A*, **634**, A30
- Neumann D. M., et al., 2001, *A&A*, **365**, L74
- Neumann D. M., Lumb D. H., Pratt G. W., Briel U. G., 2003, *A&A*, **400**, 811
- Planck Collaboration et al., 2013, *A&A*, **554**, A140
- Ryu D., Kang H., Hallman E., Jones T. W., 2003, *ApJ*, **593**, 599
- Storm E. M., Jeltema T. E., Profumo S., 2012, *ApJ*, **755**, 117
- Struble M. F., Rood H. J., 1991, *ApJS*, **77**, 363
- Thierbach M., Klein U., Wielebinski R., 2003, *A&A*, **397**, 53
- Timokhin A. N., Aharonian F. A., Neronov A. Y., 2004, *A&A*, **417**, 391
- Völk H. J., Aharonian F. A., Breitschwerdt D., 1996, *Space Sci. Rev.*, **75**, 279
- Willson M. A. G., 1970, *MNRAS*, **151**, 1
- Wood M., Caputo R., Charles E., Di Mauro M., Magill J., Perkins J. S., Fermi-LAT Collaboration 2017, in 35th International Cosmic Ray Conference (ICRC2017). p. 824 ([arXiv:1707.09551](https://arxiv.org/abs/1707.09551))
- Xi S.-Q., Wang X.-Y., Liang Y.-F., Peng F.-K., Yang R.-Z., Liu R.-Y., 2018, *Phys. Rev. D*, **98**, 063006
- Zargaryan D., Baghmany V., Aharonian F., Yang R.-Z., Casanova S., Mackey J., 2021, POS, <https://pos.sissa.it/395/582/pdf>
- Zhang C., Churazov E., Zhuravleva I., 2021, *MNRAS*, **501**, 1038
- van Weeren R. J., de Gasperin F., Akamatsu H., Brüggemann M., Feretti L., Kang H., Stroe A., Zandanel F., 2019, *Space Sci. Rev.*, **215**, 16

APPENDIX A: SIMULATIONS

To deal with the complexity of the favored disk + p_1 + p_2 + p_3 model as well as the low detection significances of the components in this model, we generated 1000 simulated datasets for the whole ROI with *simulate_roi* tool in Fermipy using the best-fitted parameters of the model as input. This tool takes the predicated number of counts for the given model and generates Poisson-distributed random (*randomize=True*) data. Then, for each simulated ROI, we performed a fitting by leaving all spectral parameters of the disk and point-like components as well as the normalization of the diffuse background models and the sources within 5° from the center of the ROI free. The distribution of spectral indices, energy fluxes, and the TS values are displayed in Figure 4. The results show that in 24% of all realizations, the homogeneous disk component was detected with $TS > 16$, while for the point-like components, the detection above $TS = 16$ is more common (34-40)%. Of all samples, only in one case were all four components in the region of the Coma cluster simultaneously detected with $TS > 16$, and in only 6% of cases were all components detected with $TS \geq 9$. To test whether the distribution of spectral indices of p_1 , p_2 , and p_3 are correlated with the disk component, we applied a standard independent 2-sample t-test. The

Table 3. Summary of the main systematic uncertainties estimated for the favored disk + p_1 + p_2 + p_3 model.

| Type | Impact on index | Impact on energy flux | Variation in TS |
|--------------------|-----------------|-----------------------|-----------------|
| IEM | | | |
| Disk | <5% | <76% | 1.9-17.5 |
| p_1 | <7% | <27% | 9.4-13.7 |
| p_2 | <8% | <28% | 4.9-10.6 |
| p_3 | <1% | <5% | 9.4-10.0 |
| Event class | | | |
| Disk | <8% | <10% | 4.9-6.4 |
| p_1 | <4% | <10% | 9.8-10.7 |
| p_2 | <6% | <12% | 14.8-16.3 |
| p_3 | <3% | <4% | 8.5-8.7 |

test showed that the spectral indices distributions of all point-like sources in the disk + p_1 + p_2 + p_3 model are highly anti-correlated in respect to the disk model with a probability of $< 9 \times 10^{-6}$.

APPENDIX B: SYSTEMATIC UNCERTAINTIES

Besides the simulations, we also estimated the main sources of systematic uncertainties on the disk + p_1 + p_2 + p_3 model according to (Xi et al. 2018), namely the Galactic interstellar emission model (IEM) and the selection of event class. For the former one, we repeated the analysis with SOURCE and CLEAN classes, which have larger effective areas at the expense of higher contamination of background events. To estimate the systematic effects due to the IEM, we employed eight alternative components of the spectral line surveys of HI and IC emission used in Acero et al. (2016) in the estimation of systematic uncertainties on the fitted properties of SNRs. For the diffuse isotropic emission, we used the same template fixing the normalization to the best-fit value found in the main analysis varying it by $(\pm 2\sigma)$ compatible with the statistical errors of the isotropic component of the main analysis. The combined systematic errors on the best-fitted spectral parameters for all components in disk + p_1 + p_2 + p_3 model are summarized in Table 3.